PHYSICAL REVIEW C **75**, 021902(R) (2007)

# Generalized emission functions for photon emission from quark-gluon plasma

S. V. Suryanarayana*
*Nuclear Physics Division, Bhabha Atomic Research Centre, Trombay, Mumbai 400 085, India*
(Received 13 June 2006; published 8 February 2007)

The Landau-Pomeranchuk-Migdal effects on photon emission from the quark-gluon plasma have been studied as a function of photon mass, at a fixed temperature of the plasma. The integral equations for the transverse vector function $[\tilde{\mathbf{f}}(\tilde{\mathbf{p}}_\perp)]$ and the longitudinal function $[\tilde{g}(\tilde{\mathbf{p}}_\perp)]$ consisting of multiple scattering effects are solved by the self-consistent iterations method and also by the variational method for the variable set $\{p_0, q_0, Q^2\}$. We considered the bremsstrahlung and the off shell annihilation (**aws**) processes. We define two new dynamical scaling variables, $x_T, x_L$, for bremsstrahlung and **aws** processes which are functions of variables $p_0, q_0, Q^2$. We define four new emission functions for massive photon emission represented by $g_T^b, g_T^a, g_L^b, g_L^a$ and we constructed these using the exact numerical solutions of the integral equations. These four emission functions have been parametrized by suitable simple empirical fits. Using the empirical emission functions, we calculated the imaginary part of the photon polarization tensor as a function of photon mass and energy.

DOI: 10.1103/PhysRevC.75.021902 PACS number(s): 12.38.Mh, 13.85.Qk, 24.85.+p, 25.75.−q

The quark gluon plasma (QGP) state is expected to be formed in the relativistic heavy ion collisions. In order to identify the plasma or a deconfined state, one needs to study the physical processes in quark matter, that can distinctly and conclusively identify this state of matter, such as parton energy loss leading to jet suppression mechanism. In this context, electromagnetic processes such as photons and dilepton emission are also considered as important signals. Photons and dileptons are emitted at various stages during plasma evolution, for an overview one may see [1–3] and the references therein. In-depth studies of photon emission processes in quark-gluon plasma were presented [4,5] including processes also from hot hadron gas [4]. Following hard thermal loops [6] (HTL) effective theory, the processes of bremsstrahlung [7] and a crossed process of off-shell annihilation called **aws** [8,9] contribute to photon emission at the two loop level. These two processes contribute at the leading order $O(\alpha\alpha_s)$ owing to the collinear singularity that is regularized by the effective thermal masses. Higher loop multiple scatterings having a ladder topology also contribute at the same order as the one and two loop processes [10,11]. These higher loop rescatterings, each giving finite decoherent correction to the two loop processes, need to be resummed. This resummation effectively implements the Landau-Pomarenchuk-Migdal (LPM) effects [12,13] arising due to rescattering of quarks in the medium during the photon formation time. This results in an integral equation of a transverse vector function for the real photons. The real photon emission rates are suppressed owing to the LPM effects [10,11]. The LPM modification of the photon spectrum is important at very low or at high photon energies [11,14].

The processes that contribute to virtual photon emission in QGP at $\alpha\alpha_s$ order [15] and the higher order corrections [16] were well studied. The processes $q\bar{q} \to g\gamma^*$, and $qg \to q\gamma^*$ contribute to photon polarization tensor at the order of $\alpha\alpha_s$ and appear as the one loop processes in the HTL method. Further considering LPM effects, photon emission from QGP as a function of photon mass was also reported [17]. For the case of virtual photons, these multiple scatterings modify the imaginary part of self-energy as a function of photon energy and momentum both. The dilepton emission rates are estimated in terms of the imaginary part of retarded photon polarization tensor, Bose-Einstein factor and $Q^2$ as given by Eq. 1 of [17], hence it suffices to study this polarization tensor.

For the case of virtual photon emission having small virtuality, the transverse vector function $\mathbf{f}(\mathbf{p}_\perp)$ is determined by the Arnold-Moore-Yaffe (AMY) equation [Eq. (1)] together with the energy transfer function $\delta E(\mathbf{p}_\perp, p_0, q_0, Q^2)$ as given in [17]. For the case of massive photon emission, this energy denominator is modified by replacing $M_\infty^2 \to M_{\rm eff} = M_\infty^2 + \frac{Q^2}{q_0^2} p_0 r_0$, where $r_0 = p_0 + q_0$. For $Q^2 > 4M_\infty^2$, this $M_{\rm eff}$ can vanish or even become negative. We solved the AMY equation for real photons by the variational method and a new method called iterations method [14]. These methods are formulated in terms of tilde variables defined in [11], accordingly, $\tilde{\mathbf{f}}(\tilde{\mathbf{p}}_\perp)$ and $\delta\tilde{E}$ are given by

$$2\tilde{\mathbf{p}}_\perp = i\delta\tilde{E}(\tilde{\mathbf{p}}_\perp, p_0, q_0, Q^2)\tilde{\mathbf{f}}(\tilde{\mathbf{p}}_\perp) + \int \frac{d^2\tilde{\ell}_\perp}{(2\pi)^2}\tilde{C}(\tilde{\ell}_\perp)[\tilde{\mathbf{f}}(\tilde{\mathbf{p}}_\perp) - \tilde{\mathbf{f}}(\tilde{\mathbf{p}}_\perp + \tilde{\ell}_\perp)], \quad (1)$$

$$\delta\tilde{E} = \frac{q_0 T}{2p_0(q_0 + p_0)}\left[\tilde{p}_\perp^2 + \kappa_{\rm eff}\right]. \quad (2)$$

In the above $\kappa_{\rm eff} = \frac{M_{\rm eff}^2}{m_D^2}$ and $\tilde{C}$ is the collision kernel taken from [18]. For virtual photons, the coupling of quarks to longitudinal mode must be considered. This results in a scalar function $g(\mathbf{p}_\perp)$ determined by an integral equation [17] given by Eq. (3). We refer to Eq. (3) as Aurenche-Gelis-Moore-Zaraket (AGMZ) equation. We will divide Eq. (3), by $m_D$ in order

*In nuclear physics journals and arXiv listings, my name used to appear as S. V. S. Sastry. Hereafter (by deleting Sastry) my name will appear as S. V. Suryanarayana. Email addresses: snarayan@barc.gov.in; suryanarayan7@yahoo.com

 

to get a dimensionless equation in tilde variables given by Eq. (4), where absorbing $1/m_D$ factor, the function $g$ is now redefined. Here, $g$ transforms as $\tilde{g}(\tilde{\mathbf{p}}_\perp) = \frac{m_D}{T} g(\mathbf{p}_\perp)$, similar to the $\mathbf{f}(\mathbf{p}_\perp)$ function. It implies that this $\tilde{g}$ is larger than $g$ of Eq. (3) by a factor $m_D$. Therefore, when the solution of Eq. (4) is used to get $\int \frac{d^2\tilde{\mathbf{p}}_\perp}{(2\pi)^2} \Re\tilde{g}(\tilde{\mathbf{p}}_\perp)$, the result will be larger than the true result [from Eq. (3)] by exactly $m_D$ factor. This problem was not present for the transverse part because $\mathbf{p}_\perp \cdot \mathbf{f}(\mathbf{p}_\perp)$ remains unchanged. Therefore to correct this anomaly, we will introduce the $\frac{1}{m_D}$ factor for the longitudinal contribution to the imaginary part of photon polarization tensor. We have solved the above Eqs. (1) and (4) by iterations and variational method [19] and compared their results, these details will be discussed elsewhere. We obtained the $\mathbf{p}_\perp$ distributions for the bremsstrahlung and **aws** cases for both transverse and longitudinal components. We considered five photon energy values, for each energy ten photon momenta and ten quark momenta, i.e., about 500 distributions for each of the transverse and longitudinal components of bremsstrahlung and **aws** processes.

$$2\sqrt{|p_0 r_0|} = i\delta E(\mathbf{p}_\perp, p_0, q_0, Q^2) g(\mathbf{p}_\perp) + g^2 C_F T \times \int \frac{d^2\ell_\perp}{(2\pi)^2} C(\ell_\perp)[g(\mathbf{p}_\perp) - g(\mathbf{p}_\perp + \ell_\perp)], \tag{3}$$

$$2\sqrt{\frac{|p_0 r_0|}{m_D^2}} = i\delta \tilde{E}((\tilde{\mathbf{p}}_\perp, p_0, q_0, Q^2)\tilde{g}(\tilde{\mathbf{p}}_\perp) + \int \frac{d^2\tilde{\ell}_\perp}{(2\pi)^2} \tilde{C}(\tilde{\ell}_\perp)[\tilde{g}(\tilde{\mathbf{p}}_\perp) - \tilde{g}(\tilde{\mathbf{p}}_\perp + \tilde{\ell}_\perp)], \tag{4}$$

$$x_0 = \frac{|(p_0+q_0)p_0|}{q_0 T}; \quad x_3 = \frac{q_0 T}{Q^2}, \tag{5}$$

$$x_1 = x_0 \frac{M_\infty^2}{m_D^2}, \tag{6}$$

$$x_2 = x_0 \frac{Q^2}{q_0 T}, \tag{7}$$

$$I_T^{b,a} = \int \frac{\mathbf{d}^2\tilde{\mathbf{p}}_\perp}{(2\pi)^2} \tilde{\mathbf{p}}_\perp \cdot \Re\tilde{\mathbf{f}}(\tilde{\mathbf{p}}_\perp), \tag{8}$$

$$I_L^{b,a} = \int \frac{\mathbf{d}^2\tilde{\mathbf{p}}_\perp}{(2\pi)^2} \Re\tilde{g}(\tilde{\mathbf{p}}_\perp), \tag{9}$$

$$g_{T,L}^{b,a}(x_{T,L}) = I_{T,L}^{b,a}(x_{T,L}) c_{T,L}^{b,a}. \tag{10}$$

In the following calculations, we have used two flavors, three colors, $\alpha_s = 0.30$ and $T = 1.0$ GeV. In Eqs. (5), (6), (7) we define four dimensionless variables. Here, the variable $x_1$ is the inverse of $x$ variable used in [14] for real photon production. $I_{T,L}^{b,a}$ are defined in Eqs. (8) and (9) which are obtained by integrating the $\mathbf{p}_\perp \cdot \mathbf{f}(\mathbf{p}_\perp)$, $g(\mathbf{p}_\perp)$ distributions (in Ref. [14] there was a 2 factor extra for $I$ as given by $2\mathbf{p}_\perp \cdot \mathbf{f}(\mathbf{p}_\perp)$. $I_{T,L}^{b,a}$ are the quantities required for the imaginary part of the polarization tensor. The superscripts $b, a$ in these equations represent bremsstrahlung or **aws** processes depending on the $p_0$ value used. The subscripts $T, L$ represent contributions from transverse $[\mathbf{f}(\mathbf{p}_\perp)]$ or longitudinal $[g(\mathbf{p}_\perp)]$ parts. Using the iterations data, we obtained the integrated values of $\mathbf{p}_\perp$ distributions as given by $I_{T,L}^{b,a}$ of Eqs. (8) and (9). We define the emission functions $g_{T,L}^{b,a}$ in Eq. (10) which are functions of variables $x_{T,L}$. These $x_{T,L}$ variables are given in Eqs. (11) and (12). The $g_{T,L}^{b,a}$ are obtained from corresponding $I_{T,L}^{b,a}$ values by multiplying with $c_{T,L}^{b,a}$ coefficient factors given in Eqs. (13)–(16). The quantities $x_{T,L}$ and $c_{T,L}^{b,a}$ in Eqs. (11)–(16) are not definitions, but are results of a search for dynamical variables hidden in the solutions of AMY and AGMZ equations:

$$x_T = x_1 + x_2, \tag{11}$$

$$x_L = x_2, \tag{12}$$

$$c_T^b = \frac{1}{x_1^2}, \tag{13}$$

$$c_T^a = \frac{1}{x_1 x_2} \tag{14}$$

$$c_T^a = c_T^b \frac{x_3}{1.0 + x_3} \quad \text{for} \quad x_2 \leqslant 2.0$$

$$c_L^b = \frac{Q^2}{(p_0(p_0+q_0))^{1.50}} \frac{(1.50 + x_3^{0.75})}{x_2^{1/3}}, \tag{15}$$

$$c_L^a = \frac{1}{x_1^{1.4} q_0^{0.5} (1 + x_3^{0.5})} x_2^{0.2}, \tag{16}$$

$$g_T^b(x) = \frac{10.0}{5.0 + 3.0\sqrt{x} + x}, \tag{17}$$

$$g_T^a(x) = \frac{0.80}{1 + (3.0/x^{1.2})} \tag{18}$$

$$g_T^a = g_T^b \quad \text{for} \quad x_2 \leqslant 2.0$$

$$g_L^b(x) = \frac{0.0876}{1 + (x/3.7727)^{1.18}} \tag{19}$$

$$g_L^a(x) = 0.2703 x^{0.65} + 0.20 x^2,$$

$$\text{if} \quad x > 2.5 \quad \text{then} \quad g_L^a(x) = 1.8 x^{0.3}. \tag{20}$$

The $I_T^b(x)$ when plotted as a function of $x_2$ variable exhibits some trends as a function of $p_0, q_0, Q^2$ values, but still does not bring out the underlying dynamical scale hidden in the data [20]. In Figure 1(a), we show the same data transformed to $g_T^b(x_T)$ as a function of $x_T (= x_2 + x_1)$ variable. The hidden scale is revealed in this plot, where data for all different $p_0, q_0, Q^2$ values merged into a single curve. This is the transverse mode bremsstrahlung emission function. Importantly, the crosses in the figure represent low $Q^2$ data for transverse mode of the **aws** process, intentionally plotted here. The empirical fit to this data (curve in figure) is given by $g_T^b(x)$ in Eq. (17). A similar exercise for transverse **aws** is shown in Fig. 1(b). The $c_T^a$ that transform the integrated values into $g$ functions are very complex. We have parametrized these data by an empirical function given in Eq. (18). For $Q^2 < 2.0$ GeV$^2$ (possibly the data for $Q^2 < 4M_\infty^2$), the data deviate from general trends as shown by crosses in Fig. 1(b). It was noticed that the same data, when transformed as required in Fig. 1(a) and plotted

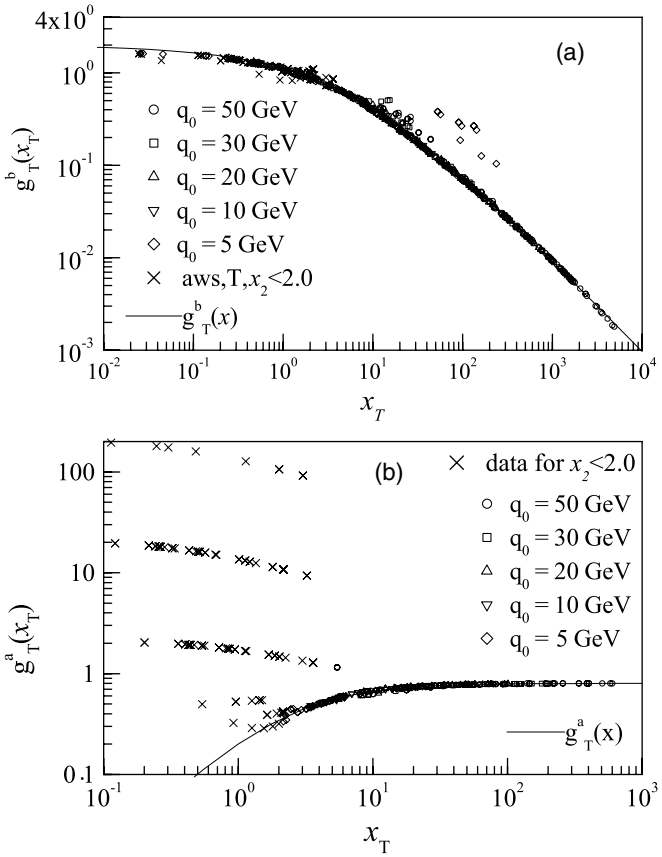


FIG. 1. (a) The dimensionless emission function $g^b_T(x)$ versus dynamical variable $x_T$ defined in Eq. (11). The symbols represent the integrated values of $\mathbf{p}_\perp$ distributions of about 500 cases of $\{p_0, q_0, Q^2\}$values and are transformed by $c^b_T$ coefficient function given in Eq. (13). Essentially, various symbols merge and can not be distinguished. The solid curve is an empirical fit given by Eq. (17). (b) The dimensionless emission function $g^a_T(x)$ versus dynamical variable $x_T$. The transformation coefficients $c^a_T$ and empirical fit are given by Eqs. (14), (18).

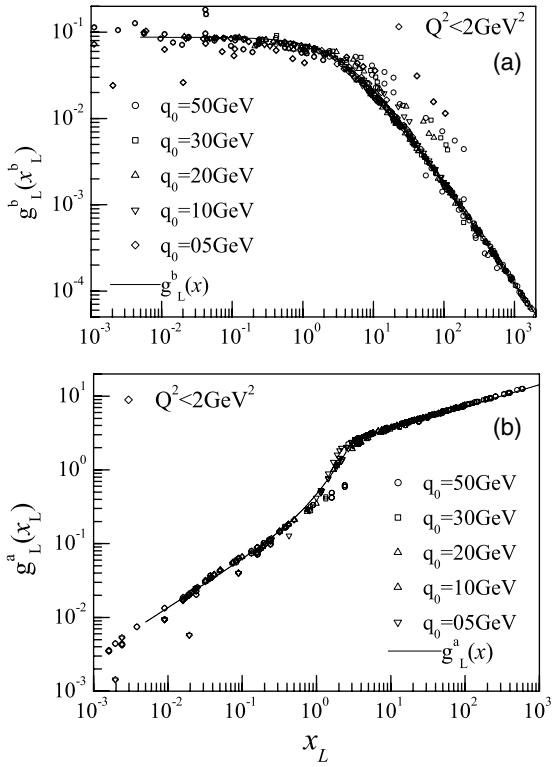


FIG. 2. (a)The dimensionless emission function $g^b_L(x)$ versus dynamical variable $x_L$ defined in Eq. (12). The transformation coefficients $c^b_L$ and empirical fit (solid curve) are given in Eqs. (15), (19). In Fig. (b) the dimensionless emission function $g^a_L(x)$ for longitudinal contribution to **aws** is shown. The $c^b_T$ and the empirical fit (solid curve) are given in Eqs. (16), (20).

versus $x_T$, are very close to the bremsstrahlung function [see crosses in Fig.1(a)].

Figure 2(a) shows the results for bremsstrahlung longitudinal component. The corresponding $c^b_L$ coefficient functions and the empirical fits represented by $g^b_L(x)$ are given in Eqs. (15) and (19). Similarly, Fig. 2(b) shows the results for the **aws** longitudinal component. The corresponding $c^a_L$, $g^a_L(x)$ are given in Eqs. (16) and (20).

The imaginary part of the retarded photon polarization tensor can be calculated using the $\mathbf{p}_\perp$ integrated values as given in Eq. 16 of [17]. Previously, we used the results from variational and iteration methods to obtain the $I^{b,a}_{T,L}$ values by integrating the distributions. We transformed these into $g^{b,a}_{T,L}$ functions shown in Figs. 1 and 2 and we fitted these by empirical functions Eqs. (17)–(20). Using the empirical functions, for any $p_0, q_0, Q^2$ values, we can generate the integrated value $I^{b,a}_{T,L}(x)$ values, circumventing the need to solve the integral equations. Thus, the imaginary part of the retarded photon polarization tensor ($\Im\Pi_R$) is calculated, as in Eq. (21). Here, the superscript $i$ denotes $\{b, a\}$ depending on the value of the integration variable $p_0$. In this Eq. (21), one should note the factor $\frac{1}{m_D}$ in the longitudinal part for reasons explained before. All terms in this equation contributing to polarization tensor are calculated and plotted in Fig. 3. The contribution of one loop processes to the imaginary part of the photon polarization tensor [15] is added to our empirical result to obtain the total result for $\Im\Pi_R$:

$$\Im\Pi^\mu_{R\mu} = \frac{e^2 N_c}{2\pi}\int_{-\infty}^{\infty} dp_0[n_F(r_0) - n_F(p_0)] \otimes (m_D^2)\left[\frac{p_0^2 + r_0^2}{2(p_0 r_0)^2}\left(\frac{g^i_T(x_T)}{c^i_T}\right) + \frac{1}{\sqrt{|p_0 r_0|}}\frac{Q^2}{q^2}\left(\frac{1}{m_D}\right)\left(\frac{g^i_L(x_L)}{c^i_L}\right)\right]. \quad (21)$$

Figure 3 shows the $\Im\Pi_R$ plotted as a function of $Q^2/T^2$ for a photon energy of 50 GeV. It can be seen that the empirical approach has predicted rather remarkably well the the results of [17] (circles in figure) over the $Q^2/T^2$ in the range of 1–100. The bremsstrahlung is insignificant because the $q_0$ is very high. The transverse component of **aws** only contributes, with a small contribution from a longitudinal component above $Q^2 > 20\,\mathrm{GeV}^2$. As shown in [17], the multiple rescatterings in the medium only marginally increase the $\Im\Pi_R$ at low $Q^2$. However, the rescattering corrections smooth out the

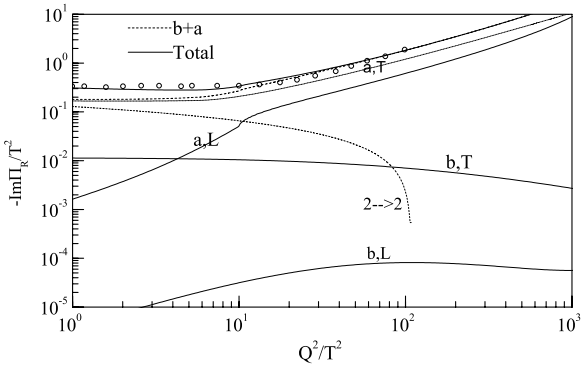


FIG. 3. $\Im\Pi_R$ plotted as a function of $Q^2/T^2$ for a photon energy of 50 GeV. The transverse components of bremsstrahlung, **aws**, the insignificant contribution from longitudinal parts, and the $2 \rightarrow 2$ processes contribution are all shown. The one loop results are obtained using the formula as given in Eq. 2.13 of [15] (as mentioned in Eq. 5.18 of [9]). The results of Fig.3 of [17] shown by circles for reference.

discontinuity at the tree level threshold $Q^2 = 4M_\infty^2$ [17]. These calculations were repeated for five photon energies [20].

In conclusion, the photon emission rates from the quark gluon plasma have been studied as a function of photon mass, considering LPM effects. The self-consistent iteration method and the variational method have been used to solve the AMY and AGMZ integral equations. We obtained the $\Re\tilde{\mathbf{f}}(\tilde{\mathbf{p}}_\perp)$, $\Re\tilde{g}(\tilde{\mathbf{p}}_\perp)$ distributions as a function of photon mass, photon energy, and quark momentum. We defined two new dynamical variables $x_T, x_L$ for transverse and longitudinal components of the bremsstrahlung and **aws** mechanism. In addition, we defined four new emission functions, namely, $g_T^b(x_T)$, $g_T^a(x_T)$, $g_L^b(x_L)g_L^a(x_L)$, and these have been constructed using the solutions of integral equations. In terms of the empirical emission functions, we have calculated the imaginary part of retarded photon polarization tensor as a function of photon energy and mass.

I thank Dr. Francois Gelis for fruitful discussions during the course of this work. I thank Profs. R. S. Bhalerao, Raghava Varma, Ajit K. Sinha, Drs. A. K. Mohanty, Alok Saxena, S. Ganesan, S. Kailas and R. K. Choudhury for discussions. Computer Division, BARC is thanked for the computational services provided.

[1] Thomas Peitzmann and Markus H. Thoma, Phys. Rep. **364**, 175 (2002); Frank D. Steffen, nucl-th/9909035.
[2] Charles Gale and K. L. Haglin, hep-ph/0306098; Charles Gale, Nucl. Phys. **A774**, 335 (2006).
[3] R. Rapp, hep-ph/0204003.
[4] J. Kapusta, P. Lichard, and D. Seibert, Phys. Rev. D **44**, 2774 (1991).
[5] R. Baier, H. Nakkagawa, A. Niegawa, and K. Redlich, Z. Phys. C **53**, 433 (1992).
[6] E. Braaten and R. D. Pisarski, Nucl. Phys. **B337**, 569 (1990).
[7] P. Aurenche, F. Gelis, R. Kobes, and E. Petitgirard, Phys. Rev. D **54**, 5274 (1996); Z. Phys. C **75**, 315 (1997).
[8] P. Aurenche, F. Gelis, H. Zaraket, and R. Kobes, Phys. Rev. D **58**, 085003 (1998); **61**, 116001 (2000).
[9] P. Aurenche, F. Gelis, and H. Zaraket, J. High Energy Phys. 07 (2002) 063; Phys. Rev. D **62**, 096012 (2000).
[10] Peter Arnold, Guy D. Moore, and Laurence G. Yaffe, J. High Energy Phys. 11 (2001) 057.
[11] Peter Arnold, Guy D. Moore, and Laurence G. Yaffe, J. High Energy Phys. 12 (2001) 009.
[12] L. D. Landau and I. Ya. Pomeranchuk, Dokl. Akad. Nauka SSR **92**, 535 (1953); **92**, 735 (1953).
[13] A. B. Migdal, Phys. Rev. **103**, 1811 (1956).
[14] S. V. S. Sastry, Phys. Rev. C **67**, 041901(R) (2003); hep-ph/0208103.
[15] T. Altherr and P. V. Ruuskanen, Nucl. Phys. **B380**, 377 (1992).
[16] M. H. Thoma and C. T. Traxler, Phys. Rev. D **56**, 198 (1997); hep-ph/9701354.
[17] P. Aurenche, F. Gelis, Guy D. Moore, and H. Zaraket, J. High Energy Phys. 12 (2002) 006.
[18] P. Aurenche, F. Gelis, and H. Zaraket, J. High Energy Phys. **05** (2002) 043.
[19] S. V. Suryanarayana, hep-ph/0609096.
[20] S. V. Suryanarayana, hep-ph/0606056.